Multi-objective Hierarchical Optimization of Interior Permanent Magnet Synchronous Machines Based on Rotor Surface Modification

Ran Xu, and Wenming Tong, *Member, IEEE*

***Abstract*—To solve the problem of large torque ripple of interior permanent magnet synchronous motor (IPMSM), the rotor surface notch design method was used for V-type IPMSM. In order to accurately obtain the optimal parameter values to improve the torque performance of the motor, this paper takes the output torque capacity and torque ripple as the optimization objectives, and proposes a multi-objective layered optimization method based on the parameter hierarchical design combined with Taguchi method and response surface method (RSM). The conclusion can be drawn by comparing the electromagnetic performance of the motor before and after optimization, the proposed IPMSM based on the rotor surface notch design can not only improve the output torque, but also play an obvious inhibition effect on the torque ripple.**

***Index Terms*—Interior permanent magnet synchronous machine, Torque ripple, Rotor surface modification, RSM, Multi-objective hierarchical optimization.**

I. INTRODUCTION

WITH the development of permanent magnet materials and the continuous improvement of their performance, permanent magnet motors have attracted wide attention[1]. IPMSM has great advantages in weak magnetic speed regulation and power density due to its asymmetrical d- and q-axes inductance and reluctance torque. It is widely used in new energy vehicles, aerospace and other fields [2-3]. However, IPMSM has the disadvantage of large torque ripple, which will cause mechanical vibration and noise of the motor, and have a great impact on its operating performance.

At present, the problem of large torque ripple of IPMSM can be weakened from two aspects: ontology optimization design and reasonable control strategy. From the perspective of control strategy, references [4]-[5] generates an additional torque by injecting harmonic current to reduce the harmonic torque component and thus reduce the torque ripple. From the perspective of motor structure improvement, references [7]-[8] forms an uneven air gap structure by changing the rotor core shape, but it increases the sinusoidal of no-load back electromotive force and also increases the average air gap length. Thus, although this method effectively weakens the torque ripple, it also reduces the output torque of the motor. In addition, skewed stator slot [6], different stator groove shapes [9], mixed pole structure [10], rotor asymmetric structure [11], rotor pole deviation [12], pole arc coefficient optimization [13]-[14], permanent magnet divided into chunks [15]and other methods can be used to reduce torque ripple.

In order to determine the optimal parameter value more accurately and further improve the electromagnetic performance of the motor, many scholars at home and abroad have introduced intelligent algorithms into the multi-objective optimization of the IPMSM. The application of Ant Colony Optimization to motor optimization design in reference [16] greatly attenuates the calculation time and improves the calculation efficiency but the influence weights between parameters are not considered. In reference [17], Taguchi method was adopted to optimize the permanent magnet slot of U-shaped rotor, which reduced the iron consumption and torque ripple of the motor. In reference [18], a method combining RSM and seagull optimization algorithm was used for multi-objective optimization of the interior motor. In reference [19], a method combining parametric hierarchical design and RSM was proposed for multi-objective optimization of the interior motor with asymmetric V-rotor structure. However, the parameters selected in references [18-19] are only limited to the rotor.

In this paper, the performances of output torque capacity and torque ripple of the motor are taken as the optimization objectives. A multi-objective layered optimization method based on the parameter hierarchical design combined with Taguchi method and RSM is applied to the surface notch design of an IPMSM. The RSM is used to optimize the parameters of the first layer, Taguchi method is used to optimize the parameters of the second layer, and univariate parameterized scanning method is used to optimize the parameters of the third layer. This method can quickly determine the optimal parameter value and greatly improve the optimization efficiency. The conclusion can be drawn by comparing the electromagnetic performance of the motor before and after optimization, the proposed IPMSM based on the rotor surface notch design can not only improve the output

Manuscript received November 23, 2022; revised December 16, 2022; accepted December 18, 2022. date of publication December 25, 2022; date of current version December 18, 2022.

This work has been supported by the Liaoning Revitalization Talents Program (XLYC2007107). (*Corresponding Author*: *Wenming Tong*)

Ran Xu is with the School of Electrical Engineering, Shenyang University of Technology, Shenyang 110870, China (e-mail: 1250287906@qq.com).

Wenming Tong is with the National Engineering Research Center for Rare Earth Permanent Magnet Machines, Shenyang University of Technology, Shenyang 110870, China (e-mail: twm822@126.com).

Digital Object Identifier 10.30941/CESTEMS.2022.00046

torque, but also play an obvious inhibition effect on the torque ripple.

II. INITIAL DESIGN OF MOTOR

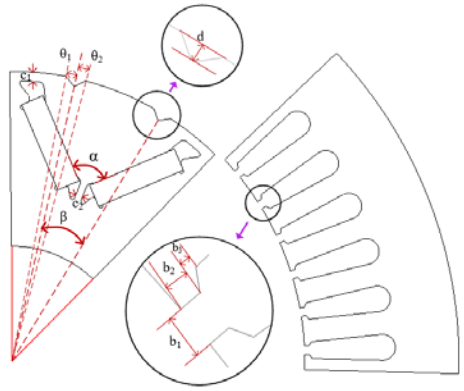

Fig. 1. Model structure of IPMSM with surface notch.

TABLE I
MOTOR PARAMETERS

Parameter	Value
Stator outer diameter /mm	194
Rotor outer diameter /mm	125.6
Axial length of moter/mm	75
Number of slots	48
Number of poles	8
Rated power/kW	20
Rated current /A	89
Rated speed /(r/min)	4500

TABLE II
INITIAL VALUE AND VARIATION RANGE OF OPTIMIZATION PARAMETERS

Parameter	Initial value	Variation range
The central angle across the lowest notch β/°	24	[15,30]
Offset angle outside the notch θ_1/°	2	[2,8]
Offset angle in notch θ_2/°	2	[1,7]
Depth of notch d/mm	0.5	[0.2,1.1]
Angle between magnetic poles α/°	90	[80,100]
The width of magnetic bridge 1 c_1/mm	2	[1.6,2.4]
The width of magnetic bridge 2 c_2/mm	1.5	[1,2]
Width of notch b_1/mm	1.8	[1.5,2.4]
Depth of notch b_2/mm	1	[0.9,1.2]
The depth of the groove shoulder angle b_3/mm	0.5	[0.4,0.7]

The research object of this paper is a traditional three-phase IPMSM with 48-slot and 8-pole. The motor parameters are shown in Table I. Fig.1 is the topological structure of the IPMSM.

The optimization variables are labeled in Fig.1. A total of 10 design variables need to be optimized by keeping the inner and outer diameter and axial length of the rotor unchanged. The variation range and initial value of related parameters are shown in Table II.

III. MULTI-OBJECTIVE OPTIMIZATION DESIGN OF MOTOR

The optimization process, as shown in Fig.2, is mainly divided into three parts: determine optimization objectives and constraints, conduct sensitivity analysis and stratification of parameters, and adopt different optimization methods according to different sensitivities.

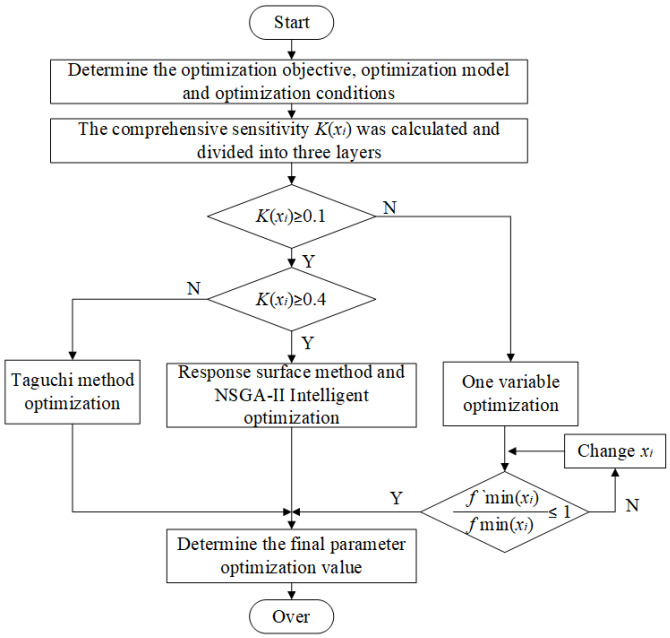

Fig.2 Flow chart of optimization

A. Determine Optimization Objectives and Constraints

This paper takes improving the average output torque and reducing the torque ripple under rated load conditions as the optimization objectives. The output torque of the motor is calculated under the control strategy of the maximum torque current ratio. Torque ripple is the ratio of the peak value of torque to the average torque, as shown in Equation (1).

$$T_{ripple} = \frac{T_{\max} - T_{\min}}{T_{avg}} \times 100\% \tag{1}$$

Where, T_{ripple}, $T_{\max}$, $T_{\min}$ and T_{avg} are respectively the torque ripple, maximum output torque, minimum output torque and average torque of the motor.

Then, the comprehensive optimization objective function is used to evaluate the motor torque performance, and the weight coefficient λ is used to represent the relative importance of the optimization objective. There is no fixed standard for determining the weight coefficient, which is usually chosen by experience [19]. The sum of the weight coefficients is 1, λ_1=λ_2=0.5 is taken to give consideration to the output torque and torque ripple.

$$\mathrm{f}_{\min}(x_i) = \lambda_1 \frac{T'_{\text{avg}}}{T_{avg}(x_i)} + \lambda_2 \frac{T'_{ripple}}{T'_{ripple}(x_i)} \tag{2}$$

$$\lambda_1 + \lambda_2 = 1 \tag{3}$$

Where, T'_{avg} and T'_{ripple} are respectively the torque output and torque ripple before optimization; $T_{avg}(x_i)$ and $T_{ripple}(x_i)$ are the optimal values of torque and torque ripple, respectively.

The constraint conditions of the motor are shown in Equation (4) :

$$\left.\begin{aligned} &T_{\text{avg}} \geq 45.0N\bullet\text{m} \\ &T_{\text{ripple}} \leq 5.0\% \\ &\min x_i \leq x_i \leq \max x_i \end{aligned}\right\} \quad (4)$$

Where, $\min x_i$ and $\max x_i$ are the minimum and maximum variation values of the design parameters respectively.

B. Parameter Sensitivity Analysis

The sensitivity index is introduced to determine the influence degree of design parameters on the optimization objective. The equation is shown in Equation (5).

$$h(x_i) = \frac{\partial f(p_i) / f(p_i)}{\partial p_i / p_i} \quad (5)$$

Where, $f(p_i)$ is the response value of the optimization target, and p_i is the design variable.

In order to comprehensively consider the two optimization objectives of average torque and torque ripple, the comprehensive sensitivity analysis index $G(x_i)$ is introduced to measure the influence degree of parameters on the motor optimization objectives. The equation is shown in Equation (6).

$$G(x_i) = \lambda_1 \left| h_{avg}(x_i) \right| + \lambda_2 \left| h_{ripple}(x_i) \right| \quad (6)$$

Where, $h_{avg}(x_i)$ and $h_{ripple}(x_i)$ are the sensitivity of design parameters to average torque and torque ripple respectively.

Based on the above analysis, the sensitivity analysis of the motor parameters is carried out, and the results are shown in Table III

TABLE III
SENSITIVITY ANALYSIS RESULTS OF PARAMETERS

Parameter	$h_{avg}(x_i)$	$h_{ripple}(x_i)$	$K(x_i)$
β	0.021	4.695	2.34
θ_1	-0.026	0.444	0.235
θ_2	-0.023	0.917	0.47
d	-0.015	0.741	0.37
α	-0.226	2.033	1.13
c_1	-0.193	0.72	0.46
c_2	-0.059	-0.013	0.036
b_1	-0.045	0.517	0.281
b_2	0.006	-0.053	0.029
b_3	0.003	-0.039	0.021

According to the comprehensive sensitivity analysis results in Table III, the parameters can be divided into three layers. The parameters with greater comprehensive sensitivity are placed in the first layer and the smaller ones in the third layer. The results are shown in Table IV.

TABLE IV
PARAMETER STRATIFICATION RESULTS

Layered	Parameter
First layer: $K(x_i) \geq 0.4$	$\beta,\theta_2,\alpha,c_1$
Second layer: $0.1 < K(x_i) < 0.4$	θ_1,d,b_1
Third layer: $K(x_i) \leq 0.1$	c_2,b_2,b_3

IV. PARAMETER HIERARCHICAL OPTIMIZATION

At present, finite element software is often used to optimize the motor design. When multiple parameters of the motor are optimized at the same time, the amount of simulation calculation of the software will be greatly increased, and the time is relatively large. Taking the 10 motor parameters in this paper as an example, when each parameter is selected at 4 levels, 4^{10}=1048576 times of simulation is required.

Therefore, this paper adopts the design concept of parameter hierarchical optimization. There are 29 sample points required for the establishment of response surface model at the first layer, 16 sample points required for Taguchi algorithm at the second layer, and 12 sample points required for univariate scanning at the third layer. A total of 57 sampling times are required, which greatly improves the efficiency of optimization design.

A. Parameter Optimization of the First Layer

In the process of optimization, there is no accurate relationship between the design parameters and the target, so this paper builds a response surface model to fit an approximate expression to predict the optimization parameters.

$$f(x_1,x_2,x_3,x_4) = \gamma_0 + \sum_{i=1}^{4}\gamma_0 x_i + \sum_{i=1}^{4}\gamma_1 x_i^2 + \sum_{i=1}^{3}\sum_{j>i}^{4}\gamma_1 x_i x_j + \varepsilon \quad (7)$$

There are two main methods to collect sample points: Box-Behnken experimental design (BBD) and central composite experimental design (CCD). Although CCD has a better fitting surface than BBD, the sampling points will exceed the original level during the sampling process. Therefore, this paper adopts BBD to collect sample points.

The simulation results of the sampled points were analyzed by Design-Expert software, and the fitting regression equation of the optimization target was obtained. The fitting equation of average torque is

$$\begin{aligned} T_{\text{avg}} =& -0.770+0.147*\beta-0.085*\theta_2+1.330*\alpha-4.722*c_1+0.007*\beta*\theta_2 \\ &-0.003*\beta*\alpha-0.017*\beta*c_1-0.028*\theta_2*c_1-0.01*\alpha*c_1 \\ &+0.004*\beta^2-0.024*\theta_2^2-0.008*\alpha^2+0.407*c_1^2 \end{aligned} \quad (8)$$

The fitting regression equation of torque ripple is

$$\begin{aligned} T_{ripple} =& -560.465+9.421*\beta+3.961*\theta_2+5.691*\alpha+197.224*c_1 \\ &-0.09*\beta*\theta_2-0.004*\beta*\alpha+0.218*\beta*c_1+0.001*\theta_2*\alpha \\ &+0.433*\theta_2*c_1-0.356*\alpha*c_1-0.202*\beta^2-0.449*\theta_2^2 \\ &-0.026*\alpha^2-41.002*c_1^2 \end{aligned} \quad (9)$$

Then, NSGA-II algorithm is used for intelligent optimization, which greatly reduces the computational complexity compared with NSGA.

Combined with the fitting equations of average torque and torque ripple, the final optimal values of the first layer parameters were determined. Table V shows the change results of parameters and optimization objectives of NSGA-II algorithm before and after optimization.

As can be seen from Table V, after optimization, the Angle between the magnetic poles is still 90°. The central angle of the notch lowest point, the offset angle in the notch and the

width of the magnetic bridge 1 are changed to 15°, 3° and 1.8mm, respectively. After optimization, the output torque is increased from the initial value of 44.65N·m to 45.35N·m, increasing by 1.6%, and the torque ripple is reduced from 23.61% to 3.89%. Moreover, the optimization results of NSGA-II algorithm are close to the finite element simulation results, which indicates the accuracy of the response surface model in predicting the results.

TABLE V
RESULTS OF NSGA-II ALGORITHM BEFORE AND AFTER OPTIMIZATION

Parameter	Before optimization	The result of the optimized algorithm	The finite element results after optimization
β/°	24	15	15
θ_2/°	2	3	3
α/°	90	90	90
c_1/mm	2	1.8	1.8
T_{avg}/(N·m)	44.65	45.40	45.35
T_{ripple}/%	23.61	4.12	3.89

B. Parameter Optimization of the Second Layer

The Taguchi method is used to optimize the motor parameters of the second layer. Firstly, the three factors are represented by A, B and C respectively for convenience, and then the horizontal configuration table of the optimization factors is determined, as shown in Table VI. Secondly, according to the principle of Taguchi method, the horizontal orthogonal table of the three optimization factors and four levels is established, as shown in Table VII Finally, the average value analysis and variance analysis are carried out on the test results, and the best combination is selected.

TABLE VI
FACTORS AND THEIR CLASSIFICATION AT DIFFERENT LEVELS

Factor	A: θ_1 (°)	B:d(mm)	C:b_1(mm)
Level I	2	0.2	1.5
Level II	4	0.5	1.8
Level III	6	0.8	2.1
Level IV	8	1.1	2.4

TABLE VII
$L_{16}(3^4)$ ORTHOGONAL TABLE

Test number	A: θ_1 (°)	B:d(mm)	C:b_1(mm)
1	I	I	I
2	I	II	II
3	I	III	III
4	I	IV	IV
5	II	I	II
6	II	II	I
7	II	III	IV
8	II	IV	III
9	III	I	III
10	III	II	IV
11	III	III	I
12	III	IV	II
13	IV	I	IV
14	IV	II	III
15	IV	III	II
16	IV	IV	I

After the establishment of the orthogonal table, the 16 groups of tests in the orthogonal table are respectively calculated by finite element analysis, and the corresponding values of the two targets to be optimized for each group of tests are obtained, as shown in Table VIII.

TABLE VIII
ORTHOGONAL TABLE RESULTS OF EACH EXPERIMENT

Test number	T_{avg}(N·m)	T_{ripple}(%)
1	46.09	7
2	45.35	3.84
3	44.61	6.28
4	43.86	9.78
5	45.65	9.32
6	45.18	7.82
7	43.54	15.45
8	43.41	17.73
9	45.03	14.3
10	43.67	15.88
11	43.83	12.01
12	42.83	15.08
13	44.24	14.3
14	43.47	10.04
15	42.77	8.35
16	42.16	7.73

After the results of each group are determined, the total mean value of each group's data is calculated firstly by:

$$M(S)=\frac{1}{n}\sum_{i=1}^{n}S(i) \tag{10}$$

Where, n is the total number of tests, i is the test number, S is the target to be optimized, and $S(i)$ is the value of the target to be optimized obtained from the i-th test.

For this optimization process, the total number of tests is 16, and the two targets to be optimized are output torque and torque ripple of the motor respectively. Equation (10) is used to solve the total average value of the two targets to be optimized respectively, and the results are shown in Table IX.

TABLE IX
TOTAL AVERAGE VALUE OF THE TARGET TO BE OPTIMIZED

S	T_{avg}(N·m)	T_{ripple}(%)
$M(S)$	44.11	10.93

After the total mean value is determined, the influence of certain level of a factor on the optimization objective function can be calculated (mean value analysis). Take the influence of level I of factor A on the average torque T_{avg} as an example

The average value can be calculated by equation (11):

$$M_{A(I)}(T_{avg})=\frac{1}{4}[T_{avg}(1)+T_{avg}(2)+T_{avg}(3)+T_{avg}(4)] \tag{11}$$

Where, $M_{A(I)}(T_{avg})$ is the average value of the level i of

factor A and the correlation term of average torque T_{avg}, $T_{avg}(1)$, $T_{avg}(2)$, $T_{avg}(3)$ and $T_{avg}(4)$ are the corresponding T_{avg} of the test related to level i of factor A.

Formula (11) can be used to calculate the average value of each level of each factor about the two targets to be optimized, as shown in Table X.

TABLE X
Average values of each level for each factor

Test number	Level	T_{avg}(N·m)	T_{ripple}(%)
Factor A	I	44.98	6.73
	II	44.45	12.58
	III	43.84	14.32
	IV	43.16	10.11
Factor B	I	45.25	11.23
	II	44.42	9.4
	III	43.69	10.52
	IV	43.07	12.58
Factor C	I	44.32	8.64
	II	44.15	9.15
	III	44.13	12.09
	IV	43.83	13.85

The variance calculation process is expressed by:

$$S_X = \frac{\sum_{j=1}^{Q}(M_{X(j)}(S) - M(S))}{Q} \tag{12}$$

Where, $M_{A(I)}(S)$ is the average value of j level of factor X, and Q is the number of experiments, and its value is 4.

Formula (12) is used to calculate the variance of each factor to the two optimization objectives. The results are given in Table XI. These variance values reflect the relative importance of each factor to T_{avg} and T_{ripple}.

TABLE XI
Variance calculation results

Factor of optimization	T_{avg} (N·m)		T_{ripple}(%)	
	variance (10^{-2})	ratio (%)	variance (10^{-1})	ratio (%)
A	46.2	39.95	81.32	57.95
B	66.34	57.36	13.3	9.48
C	3.11	3.69	45.71	32.57

According to the analysis of variance data in Table Ⅹ I, the influence on T_{avg} in descending order is BAC, while the influence on T_{ripple} in descending order is ACB. It can be seen that factor B has a greater influence on T_{avg}. Therefore, when selecting the level of factor B, emphasis should be placed on its influence on T_{avg}, so level I should be selected for factor B. But considering the difficulty of actual manufacturing, B chooses level II. Similarly, the selection of factor A should focus on its influence on T_{ripple}, and the selection of factor C should focus on its influence on T_{ripple}. Therefore, the final selection combination is A(I)B(II)C(I).

C. Parameter Optimization of the Third Layer

For parameters of the third layer, the univariate parameterization method can be used. It is necessary to introduce the optimization criterion judgment function. If it does not meet the requirements, the value of x_i will be changed until it meets the requirements. The standard function of judgment is

$$\frac{f'_{min}(x_i)}{f_{min}(x_i)} \le 1 \tag{13}$$

Table XII shows the comparison of results before and after scanning of parameters of the third layer. After optimization, the depth of the notch, the depth of the groove shoulder and the width of magnetic bridge 2 are 1.2mm, 0.7mm and 1.25mm, respectively. After optimization, the output torque is increased to 46.2N·m, and the torque ripple is reduced to 3.34%.

TABLE XII
Results of parameters with low sensitivity before and after optimization

Parameter	Before optimization	After optimization
b_2/mm	1	1.2
b_3/mm	0.5	0.7
c_2/mm	1.5	1.25
T_{avg}/(N·m)	45.59	46.2
T_{ripple}/%	3.45	3.34

V. COMPARATIVE ANALYSIS OF ELECTROMAGNETIC PERFORMANCE OF MOTOR BEFORE AND AFTER OPTIMIZATION

In order to verify the reliability and effectiveness of the proposed optimization method, the electromagnetic performance of the motor before and after optimization is compared and analyzed.

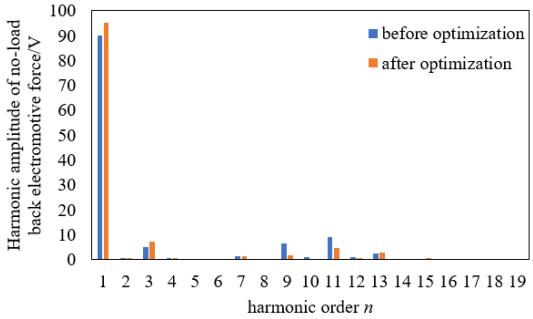

Fig. 4. Fourier analysis of no-load back EMF.

At rated speed, Fourier analysis is performed on the no-load back EMF of the motor before and after optimization, as shown in Fig. 4. It can be seen that the optimized fundamental amplitude increases from 90.1V to 95.1V.

According to the expression of torque ripple in reference [12], the $(10m \pm 1)th$ harmonics of the air gap flux density produce torque ripple, among which the 9th and 11th harmonics are the most important. Fig. 5 shows Fourier analysis of no-load radial airgap flux density before and after optimization. It can be seen that after optimization, the amplitude of the 9th harmonic decreases from 0.081T to 0.023T, and the amplitude

of the 11th harmonic decreases from 0.077T to 0.058T. It is obvious that the torque ripple can be significantly reduced after optimization.

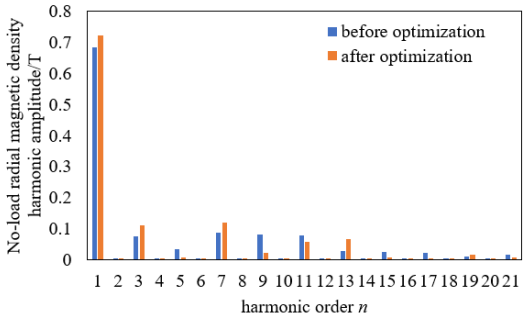

Fig. 5. No-load radial air-gap flux density' fourier analysis.

Fig.6 shows the torque curve before and after the motor optimization. After optimization, the output torque is increased from the initial value of 44.65N·m to 46.2N·m, an increase of 3.5%, and the torque ripple was reduced from 23.61% to 3.34%, a reduction of 85.9%.

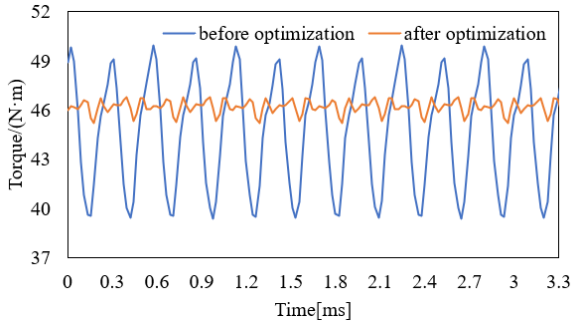

Fig. 6. Comparison of torque waveform.

VI. Experimental Verification of Prototype

In order to verify the accuracy of finite element calculation, an existing prototype of the initial IPMSM is tested. Fig.7 shows the outline of the initial IPMSM prototype and Fig.8 shows the experimental platform.

Fig.7 Appearance of the prototype.

Fig. 9(a) shows the comparison of the back EMF waveforms of the prototype obtained by finite element method and experiment. According to the spectrum shown in Fig. 9(b), there is little difference between the simulation and the test. Fig.10 shows the comparison of measured and simulated output torques under different input currents. As can be seen from Fig.9 and Fig.10, there is a slight deviation between the

Fig. 8. Experimental platform.

measured results and the finite element analysis results, but it is within the acceptable experimental error range.

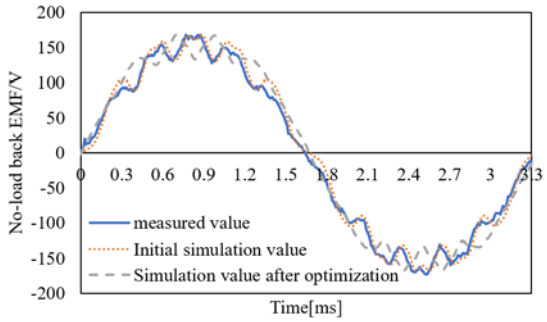

(a)Back electromotive force

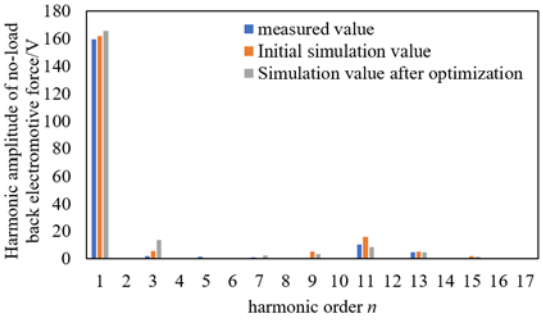

(b) Fourier analysis

Fig. 9 Measured and simulated back electromotive force and its Fourier analysis.

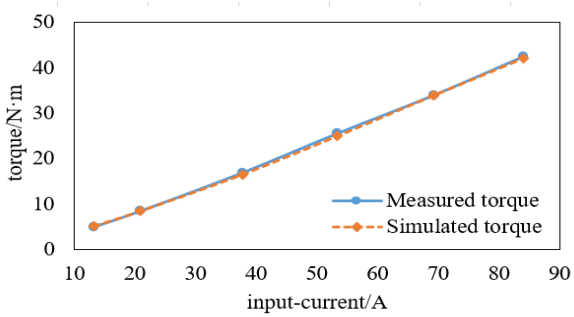

Fig.10 Measured and simulated output torque changes when input different current values.

VII. Conclusion

In this paper, a multi-objective layered optimization method for V-type IPMSM with the rotor surface notch is proposed. In order to reduce the torque ripple and improve the output torque at the same time, the comprehensive sensitivity analysis

of the structural parameters of the motor is carried out. Different comprehensive sensitivity parameters are stratified. The multi-objective hierarchical optimization method combining Taguchi method and RSM is used to find the optimal parameter values for different layers. Then the finite element method is used to optimize the simulation and compare the electromagnetic performance before and after optimization. The results show that the torque ripple is reduced by 85.9% and the output torque is increased by 3.5%.

REFERENCES

[1] J. Zheng , Y. Dai and J.Shi, "Electromagnetic noise characteristics of permanent magnet synchronous motor applied in electric vehicle," *Transactions of China Electrotechnical Society*, vol. 31, no. S1, pp. 53-59, 2016.

[2] T. Chen and J. Shan, "Distributed Control of Multiple Flexible Manipulators With Unknown Disturbances and Dead-Zone Input," *IEEE Transactions on Industrial Electronics*, vol. 67, no. 11, pp. 9937-9947, Nov 2020.

[3] Y. Fan and C. Tan, "Analysis of electromagnetic performance and principles in inserted consequent-pole permanent magnet synchronous machines," *Transactions of China Electrotechnical Society*, vol. 33, no. 11, pp. 2414-2422, 2018.

[4] G. -H. Lee, S. -I. Kim, J. -P. Hong and J. -H. Bahn, "Torque Ripple Reduction of Interior Permanent Magnet Synchronous Motor Using Harmonic Injected Current," *IEEE Transactions on Magnetics*, vol. 44, no. 6, pp. 1582-1585, June 2008.

[5] Y. Liao, S. Zhen, R.Liu and J.Yao, "Torque ripple suppression of permanent magnet synchronous motor by the harmonic injection," *Proceedings of the CSEE*, vol. 31, no. 21, pp. 119-127, 2011.

[6] Z. Q. Zhu and D. Howe, "Influence of design parameters on cogging torque in permanent magnet machines," *IEEE Transactions on Energy Conversion*, vol. 15, no. 4, pp. 407-412, Dec. 2000.

[7] Y. -H. Jung, M. -R. Park and M. -S. Lim, "Asymmetric Rotor Design of IPMSM for Vibration Reduction Under Certain Load Condition," *IEEE Transactions on Energy Conversion*, vol. 35, no. 2, pp. 928-937, June 2020.

[8] S. Zhu, Y. Hu, C. Liu and B. Jiang, "Shaping of the Air Gap in a V-Typed IPMSM for Compressed-Air System Applications," *IEEE Transactions on Magnetics*, vol. 57, no. 2, pp. 1-5, Feb. 2021.

[9] H. -C. Liu, H. -J. Lee, H. -S. Seol, S. Cho, J. Lee and Y. J. Oh, "Optimal Slot Design of IPMSM in Railway With Independently Rotating Wheelsets," *IEEE Transactions on Magnetics*, vol. 55, no. 2, pp. 1-4, Feb. 2019.

[10] W. Cui, L. Ren, J. Zhou and Q. Zhang, "A New IPMSM With Hybrid Rotor Structure for Electrical Vehicle With Reduced Magnet Loss," *IEEE Transactions on Magnetics*, vol. 58, no. 2, pp. 1-6, Feb. 2022.

[11] G. Liu, L. Liu, Q. Chen and W. Zhao, "Torque Calculation of Five-Phase Interior Permanent Magnet Machine Using Improved Analytical Method," *IEEE Transactions on Energy Conversion*, vol. 34, no. 2, pp. 1023-1032, June 2019.

[12] Q. Chen, G. Xu, G. Liu, W. Zhao, L. Liu and Z. Lin, "Torque Ripple Reduction in Five-Phase IPM Motors by Lowering Interactional MMF," *IEEE Transactions on Industrial Electronics*, vol. 65, no. 11, pp. 8520-8531, Nov. 2018.

[13] Sang-Moon Hwang, Jae-Boo Eom, Yoong-Ho Jung, Deug-Woo Lee and Beom-Soo Kang, "Various design techniques to reduce cogging torque by controlling energy variation in permanent magnet motors," *IEEE Transactions on Magnetics*, vol. 37, no. 4, pp. 2806-2809, July 2001.

[14] N. Bianchi and S. Bolognani, "Design techniques for reducing the cogging torque in surface-mounted PM motors," *IEEE Transactions on Industry Applications*, vol. 38, no. 5, pp. 1259-1265, Sept.-Oct. 2002.

[15] Y. Yang, X. Wang, C. Zhu and C. Huang, "Reducing cogging torque by adopting isodiametric permanent magnet," *2009 4th IEEE Conference on Industrial Electronics and Applications*, pp. 1028-1031,2009.

[16] Y. Qin and Z. Liang, "New progress of the ant colony algorithm in research and applications," *Computer Engineering&Science*, vol. 41, no. 01, pp. 173-184, 2019.

[17] C. Xia, L. Guo, Z. Zhang, T. Shi and H. Wang, "Optimal Designing of Permanent Magnet Cavity to Reduce Iron Loss of Interior Permanent Magnet Machine," *IEEE Transactions on Magnetics*, vol. 51, no. 12, pp. 1-9, Dec. 2015.

[18] K. Sun and S. Tian, "Multiobjective Optimization of IPMSM With FSCW Applying Rotor Notch Design for Torque Performance Improvement," *IEEE Transactions on Magnetics*, vol. 58, no. 5, pp. 1-9, May 2022.

[19] G. Liu, Y.Wang and Q. Chen, "Multi-objective optimization of an asymmetric V-shaped interior permanent magnet synchronous motor," *Transactions of China Electrotechnical Society*, vol. 33, no. S2, pp. 385-393, 2018.

Ran Xu was born in Liaoning, China. He received the B.S. degree in electrical engineering from Shenyang University of Technology, Shenyang, China, in 2021.He is currently working toward the M.S. degree in electrical engineering with the Shenyang University of Technology, Shenyang, China.

His main research interests include multi-physical field simulation and optimization of permanent magnet machines.

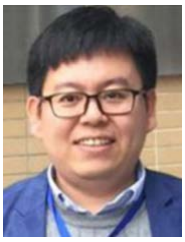

Wenming Tong (M'18) was born in Dandong, China. He received the B.S. and Ph.D. degrees in electrical engineering from the Shenyang University of Technology, Shenyang, China, in 2007 and 2012, respectively. He is currently a Professor with the National Engineering Research Center for Rare Earth Permanent Magnet Machines, Shenyang University of Technology.

His major research interests include the design, analysis, and control of hiIgh-speed and low-speed direct drive permanent magnet machines, axial flux permanent magnet machines, hybrid excitation machines, and high-performance machines with new types of soft magnetic materials.